Draft version February 2, 2021
Typeset using LaTeX **twocolumn** style in AASTeX63

Searching for Low-mass Population III Stars Disguised as White Dwarfs

Vedant Chandra [1] and Kevin C. Schlaufman [1]

[1] *Department of Physics and Astronomy*
Johns Hopkins University
3400 N Charles St
Baltimore, MD 21218, USA

(Received October 15, 2020; Revised January 29, 2021)

Submitted to AAS Journals

ABSTRACT

It is uncertain whether or not low-mass Population III stars ever existed. While limits on the number density of Population III stars with $M_* \approx 0.8\ M_\odot$ have been derived using Sloan Digital Sky Survey (SDSS) data, little is known about the occurrence of Population III stars at lower masses. In the absence of reliable parallaxes, the spectra of metal-poor main sequence (MPMS) stars with $M_* \lesssim 0.8\ M_\odot$ can easily be confused with cool white dwarfs. To resolve this ambiguity, we present a classifier that differentiates between MPMS stars and white dwarfs based on photometry and/or spectroscopy without the use of parallax information. We build and train our classifier using state-of-the-art theoretical spectra and evaluate it on existing SDSS-based classifications for objects with reliable Gaia DR2 parallaxes. We then apply our classifier to a large catalog of objects with SDSS photometry and spectroscopy to search for MPMS candidates. We discover several previously unknown candidate extremely metal-poor (EMP) stars and recover numerous confirmed EMP stars already in the literature. We conclude that archival SDSS spectroscopy has already been exhaustively searched for EMP stars. We predict that the lowest-mass primordial-composition stars will have redder optical-to-infrared colors than cool white dwarfs at constant effective temperature due to surface gravity-dependent collision-induced absorption from molecular hydrogen. We suggest that the application of our classifier to data produced by next-generation spectroscopic surveys will set stronger constraints on the number density of low-mass Population III stars in the Milky Way.

Keywords: Chemically peculiar stars (226) — Low mass stars (2050) — Population II stars (1284) — Population III stars (1285) — Sky surveys (1464) — White dwarf stars (1799)

1. INTRODUCTION

The first generation of stars formed in the Universe was made of only the stable products of Big Bang nucleosynthesis: hydrogen, helium, and a tiny amount of lithium. These Population III stars are predicted to start forming around 100 Myr after the Big Bang (e.g., Bromm 2013; Glover 2013; Greif 2015). The earliest Population III star formation calculations suggested that inefficient cooling would require large Jeans masses and therefore that Population III stars would form with a characteristic stellar mass $M_* \sim 100\ M_\odot$ (e.g., Silk 1983; Tegmark et al. 1997; Bromm et al. 1999, 2002; Abel et al. 2000, 2002). However, more recent simulations have shown that fragmentation in the accretion disks around massive Population III protostars could potentially form pristine stars at much lower masses (e.g., Stacy et al. 2010, 2012, 2016; Clark et al. 2011a,b; Greif et al. 2011, 2012; Stacy & Bromm 2013, 2014; Dopcke et al. 2013; Riaz et al. 2018; Wollenberg et al. 2020). While it is theoretically uncertain if these fragments survive or merge with the more massive protostar growing at the center of their parent accretion disk (e.g., Hirano & Bromm 2017), there is at least circumstantial observational evidence to suggest that they might sur-

Corresponding author: Vedant Chandra
vchandra@jhu.edu

vive (Schlaufman et al. 2018). If these fragments do avoid merging, then low-mass Population III stars might persist to the present day in the local Universe.

While no Population III star has been directly observed to date, according to the latest Stellar Abundances for Galactic Archaeology (SAGA) database observational searches have instead found more than 500 extremely metal-poor (EMP) stars with metallicity [Fe/H] $\lesssim -3$ (Suda et al. 2008, 2011, 2017; Yamada et al. 2013). The chemical abundances of these extreme Population II stars can be used to infer the properties of Population III stars (e.g., Hartwig et al. 2015; Placco et al. 2016; Fraser et al. 2017; Ishigaki et al. 2018; Hansen et al. 2020), as well as the early chemical evolution of the Milky Way (e.g., Beers & Christlieb 2005; Frebel & Norris 2015; Kobayashi et al. 2020).

Because stars with bright apparent magnitudes are more easily studied than stars with faint apparent magnitudes, aside from early examples found in studies of high proper motion stars (e.g., Ryan & Norris 1991a,b; Ryan et al. 1991) the vast majority of metal-poor stars studied in detail to date are at least as luminous as the main sequence turnoff (Yong et al. 2013; Cohen et al. 2013; Roederer et al. 2014). Of the 8419 unique stars in the SAGA database with effective temperature $T_{\rm eff}$ and surface gravity $\log g$ inferences, only 199 or 2.3% have $T_{\rm eff} \lesssim 6000$ K and $\log g \gtrsim 4.6$ indicative of metal-poor main sequence (MPMS) stars. As a result, only a small fraction of the Milky Way's metal-poor stellar population has been characterized to date. Indeed, assuming the PARSEC version 1.2S evolutionary tracks (Bressan et al. 2012; Chen et al. 2014, 2015) and a Kroupa (2001, 2002) initial mass function for a 10 Gyr stellar population, the luminosity function for stars with [Fe/H] ≈ -2.2 indicates that for every metal-poor turnoff star with $T_{\rm eff} \gtrsim 6000$ K and $3.8 \lesssim \log g \lesssim 4.6$ there are about 20 MPMS stars with $T_{\rm eff} \lesssim 6000$ K and $\log g \gtrsim 4.6$ in the same volume.

One significant obstacle to the identification of MPMS stars is that the optical spectra of metal-poor (and metal-free) main sequence stars are virtually indistinguishable from the optical spectra of more numerous cool hydrogen-atmosphere white dwarfs (WD). While a significant fraction of white dwarf photospheres are externally seeded with metals by ongoing accretion from circumstellar disks (e.g., Gänsicke et al. 2012; Koester et al. 2014), the high surface gravities of white dwarfs cause metals to rapidly sink out of their photospheres via gravitational settling (Schatzman 1948). The spectra of most white dwarf photospheres are therefore very similar to those of metal-free stars, featuring strong Balmer lines and possibly other absorption features due to molecular hydrogen. While in the absence of precise parallaxes it is sometimes possible to separate MPMS stars from white dwarfs using reduced proper motion as an analog for absolute magnitude (e.g., Luyten 1922), reduced proper motions are ambiguous for individual stars and can be confounded if the samples of interest belong to distinct kinematic populations.

The traditional method to distinguish MPMS stars from white dwarfs has been to visually identify MPMS stars on the basis of their narrower Balmer absorption lines at a given photometric color (Kepler et al. 2019). This process is prone to human error and very difficult for large data sets. These problems have historically been aggravated by imperfect models for the atmospheres of cool white dwarfs (Kepler et al. 2019). Recent advances have improved the fidelity of atmosphere models for white dwarfs with $T_{\rm eff} \lesssim 5000$ K (Blouin et al. 2018a,b), facilitating a theoretical comparison between MPMS star and white dwarf spectra at the coolest temperatures where spectroscopic data are currently lacking.

Tens of thousands of spectra with weak or non-existent metal lines produced by either cool white dwarfs or metal-poor/metal-free main sequence stars will be collected by ongoing and next-generation spectroscopic facilities/surveys like the Large Sky Area Multi-Object Fibre Spectroscopic Telescope (LAMOST; Cui et al. 2012), the Dark Energy Spectroscopic Instrument (DESI; DESI Collaboration et al. 2016), the fifth phase of the Sloan Digital Sky Survey (SDSS-V; Kollmeier et al. 2017), and the WHT Enhanced Area Velocity Explorer (WEAVE; Dalton et al. 2012). The volume of data produced by these ongoing and future surveys will make it impossible to rely on the traditional human classification of MPMS stars and white dwarfs. This implies that there is a need for an automated way to differentiate between MPMS stars and white dwarfs.

In this paper, we develop an automated framework to identify MPMS stars in large spectroscopic surveys with a focus on the problem of differentiating MPMS stars from spectroscopically similar white dwarfs. We describe in Section 2 state-of-the-art theoretical spectra for both MPMS stars and white dwarfs. We then introduce the Sloan Digital Sky Survey (SDSS) photometric and spectroscopic data for MPMS stars and white dwarfs securely classified using Gaia Data Release 2 (DR2) parallaxes that we use to validate and test our methods. We outline our classification algorithm in Section 3, including our extraction of features from photometric and spectroscopic observables and the validation of our classifier. In Section 4 we perform a search for candidate extremely metal-poor stars in a sample of

possible MPMS stars with SDSS photometry and spectroscopy. We review our results and their implications in Section 5. We conclude by summarizing our findings in Section 6.

2. DATA

Our goal is to differentiate MPMS stars from white dwarfs on the basis of photometry and spectroscopy alone. While there is enough observational data for MPMS stars and white dwarfs with $T_{\rm eff} \gtrsim 6000$ K, the relative faintness of MPMS stars and white dwarfs with $T_{\rm eff} \lesssim 6000$ K has resulted in few examples in the SDSS spectroscopic archive. Even though these cool MPMS stars and white dwarfs were largely out of reach of the Sloan Foundation 2.5 m Telescope, spectroscopic surveys using 4 m class telescopes like DESI will target many cool MPMS stars and white dwarfs. It is therefore necessary for us to use both theoretical spectra for cool MPMS stars and white dwarfs and empirical spectra for warmer MPMS stars and white dwarfs to train and validate our classifier. We describe those data in the following two subsections.

2.1. *Theoretical Spectra*

We first construct grids of theoretical spectra for white dwarfs and MPMS stars using state-of-the-art models. We consider temperatures in the range 4000 K $\leq T_{\rm eff} \leq$ 8000 K in 40 K steps. For each temperature, we generate white dwarf spectra with $7 \leq \log g \leq 9$ and MPMS star spectra with $3.5 \leq \log g \leq 5.5$ in steps of 0.5 dex. This procedure results in grids of 505 theoretical spectra that we use to train our classifier. For the white dwarfs, our grid of theoretical spectra is described in Blouin et al. (2018a,b). These spectra were computed assuming pure-hydrogen atmospheres, no magnetic fields, and metal-free photospheres. Blouin et al. (2018a,b, 2019) describe the improved equation of state and radiative opacities featured in this new generation of models that are especially important for cool white dwarfs with $T_{\rm eff} \lesssim 5000$ K. For MPMS stars, we use theoretical spectra computed with the PHOENIX code (Husser et al. 2013). Those models cover a broad range of temperatures and surface gravities and include metallicities $-4.0 \leq$ [Fe/H] $\leq +1.0$ and α abundances $-0.2 \leq$ [α/Fe] $\leq +1.2$. In our theoretical grid of MPMS star spectra, we use the [Fe/H] $= -4.0$ spectra with solar α abundances. The spectroscopic classifier we describe in Section 3 relies on Balmer lines, so the assumed metallicity has only a negligible impact on our analyses.

For both the MPMS and WD grids of theoretical spectra spanning $T_{\rm eff}$ and $\log g$, we tri-linearly interpolate the logarithm of the fluxes with respect to effective temperature, surface gravity, and the logarithm of wavelength. We convolve all theoretical spectra to match an instrumental resolution of 1.5 Å, comparable to the resolution of large-scale spectroscopic surveys like the SDSS, LAMOST, and DESI. We illustrate some sample theoretical spectra in Figure 1.

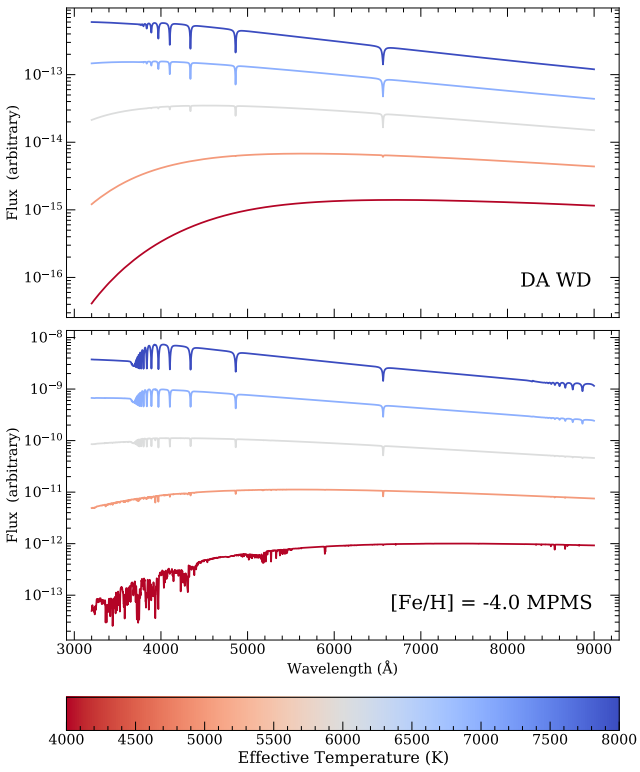

Figure 1. Sample theoretical white dwarf and MPMS star spectra from the Blouin et al. (2018a) and PHOENIX (Husser et al. 2013) libraries, respectively. We plot spectra spanning the range 4000 K $\leq T_{\rm eff} \leq$ 8000 K assuming $\log g = 8$ and $\log g = 4.5$ for the white dwarf and MPMS star spectra, respectively. For the MPMS star spectra, we assume [Fe/H] $= -4.0$ with scaled solar abundances. We offset the fluxes vertically for visual clarity. The optical spectrum of a very low-mass Population III star would be spectroscopically indistinguishable from the $T_{\rm eff} = 4000$ K white dwarf in the top panel.

2.2. *SDSS Data*

Our empirical data for warmer MPMS stars and white dwarfs come mostly from SDSS DR16 (Ahumada et al. 2020). They were collected during the first four phases of the SDSS (York et al. 2000; Eisenstein et al. 2011; Blanton et al. 2017), including its Sloan Extension for Galactic Understanding and Exploration (SEGUE), Baryon Oscillation Spectroscopic Survey (BOSS), and extended BOSS (eBOSS) programs (Yanny et al. 2009; Dawson et al. 2013, 2016). The data were collected using the Sloan Foundation 2.5 m Telescope and its imager and

optical spectrographs (Gunn et al. 1998, 2006; Doi et al. 2010; Smee et al. 2013) then placed on the SDSS photometric system using the methods described in Fukugita et al. (1996), Smith et al. (2002), and Padmanabhan et al. (2008). We also make use of Gaia DR2 astrometry (Gaia Collaboration et al. 2016, 2018; Salgado et al. 2017; Arenou et al. 2018; Lindegren et al. 2018; Luri et al. 2018; Marrese et al. 2019). We de-redden the SDSS *ugriz* magnitudes using the `mwdust` utility (Bovy et al. 2016) and the combined dust maps of Drimmel et al. (2003), Marshall et al. (2006), and Green et al. (2019).

We focus on the MPMS star and white dwarf classifications provided by Kepler et al. (2019). Those authors examined 500,000 SDSS spectra plausibly produced by white dwarfs. They provide classifications for 37,053 spectra based on 11 criteria, of which 15,716 were classified as DA white dwarfs and 15,855 were classified as subdwarf A or sdA stars (i.e., likely MPMS stars). Among the white dwarfs, over 78% were classified as DA white dwarfs with hydrogen-rich atmospheres on the basis of broad Balmer absorption lines with no other strong spectral features. Kepler et al. (2019) visually differentiated these DA white dwarfs from subdwarf A stars based on the fact that DA white dwarfs have broader Balmer lines at a given photometric color due to their high surface gravities and increased pressure broadening. Together these two classes comprise more than 85% of the classifications provided in Kepler et al. (2019).

We use in our analysis only those white dwarfs or MPMS stars classified by Kepler et al. (2019) as members of their "DA", "sdA", or "sdA/F" classes. The class "DA" designates hydrogen-atmosphere white dwarfs, the class "sdA" refers to subdwarf A stars, and the class "sdA/F" indicates ambiguous subdwarf A or F stars. This limits our sample to 14,522 spectra with prominent Balmer lines and no strong metal features. It also removes other white dwarf spectral types like helium-rich DB white dwarfs. While most of the stars classified as "sdA" or "sdA/F" stars are likely MPMS stars (e.g., Brown et al. 2017; Pelisoli et al. 2018b,a), a very small fraction could also be extremely low-mass (ELM) white dwarfs (e.g., Kosakowski et al. 2020).

As we argued above, visually separating MPMS stars from white dwarf is prone to error, especially at cool temperatures where MPMS star and white dwarf spectra are visually similar. For that reason, Kepler et al. (2019) appealed to Gaia DR2 parallaxes to distinguish MPMS stars and DA white dwarfs. At a given color, white dwarfs are far less luminous than MPMS stars due to their smaller radii. A high-quality parallax measurement therefore provides accurate classifications via absolute magnitudes. However, only about 15% of the

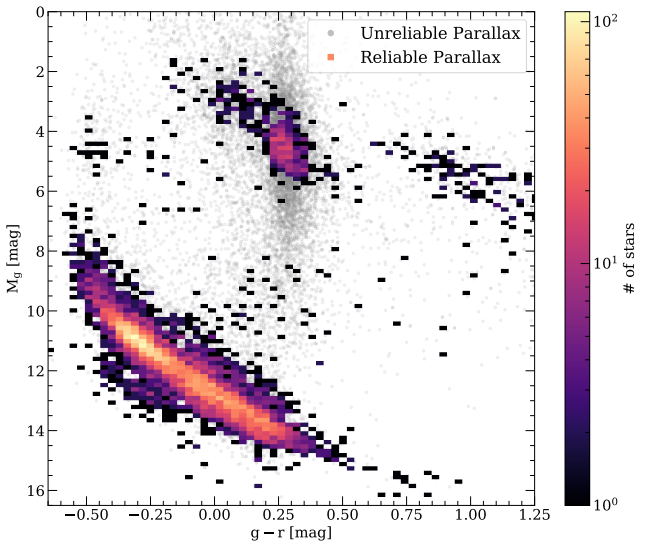

Figure 2. Color–magnitude diagram of the stars classified by Kepler et al. (2019) as white dwarfs or subdwarf A stars based on SDSS spectroscopy. Stars with unreliable parallaxes—75% of the sample—are not included in the 2D histogram and are plotted in gray. There is a clear separation between the white dwarf track on the bottom left and the more luminous stellar main sequence at the top. While it is trivial to discriminate between white dwarfs and MPMS stars when parallaxes are available, most of the Kepler et al. (2019) sample lacks reliable parallaxes in Gaia DR2.

14,522 stars in this sample have reliable parallaxes (i.e., $\pi/\sigma_\pi > 10$). As a result, the MPMS star and white dwarf classification cannot be confirmed for most of this sample. Consequently, when validating our methods we only use those stars for which a definite classification can be made based on a high-quality Gaia DR2 parallax. We require (1) `parallax_over_error > 10`, (2) `visibility_periods_used > 8`, and (3) `astrometric_sigma5d_max < 1`. This results in an empirical validation sample of 1807 stars with reliable MPMS star/white dwarf classifications. Of these, 65% are classified as DA white dwarfs and the remaining 35% are classified as MPMS stars. We illustrate this empirical validation sample in the Sloan color–magnitude diagram depicted in Figure 2.

3. METHODS

Even though visual classifications have been sufficient to separate MPMS stars from white dwarfs in the past, the volume of data expected to be produced by ongoing and next-generation spectroscopic surveys will make the traditional approach impractical. We therefore use the grids of theoretical spectra described in Section 2.1 to build an automated process to differentiate MPMS stars from white dwarfs using photometric and spectroscopic

observables alone without appealing to accurate parallax measurements. We then validate our classifier using the empirical labels in Section 2.2.

3.1. *Balmer Lines*

Both relatively warm MPMS stars and white dwarfs exhibit strong Balmer lines in their spectra. On this basis, in the absence of high-quality parallaxes MPMS stars have usually been differentiated from white dwarfs based on Balmer lines for temperatures $T_{\rm eff} \gtrsim 6000$ K. As we described above, MPMS stars have narrower Balmer lines than white dwarfs at a given temperature (Kepler et al. 2019). We now quantify this difference across several Balmer lines at once and use it to produce a rigorous selection function.

For each spectrum in the theoretical grids described in Section 2.1 we fit each of the Balmer absorption lines Hα, Hβ, Hγ, and Hδ with a Voigt profile[1]. From each profile we derive two summary statistics: the full-width at half-maximum (FWHM) in angstroms and the minimum of the profile in continuum-normalized flux units that we define as the line amplitude. For each spectrum we therefore derive eight line statistics in total which together quantify the phase space of the Balmer lines. This results in a vector of eight Balmer features per spectrum plus a "label" identifying it as the spectrum of a MPMS star or white dwarf. Our classifier then makes use of all eight features to differentiate MPMS stars from white dwarfs. We focus on Hα, Hβ, Hγ, and Hδ in this study because Balmer lines bluer than Hδ occur in lower signal-to-noise ratio regions of the SDSS spectra of cool stars.

We illustrate in Figure 3 two 2D "slices" through the Balmer line phase space that demonstrate why Balmer line features are useful for classification. Because of the faintness of cooler white dwarfs, most white dwarfs targeted by the SDSS have $T_{\rm eff} \gtrsim 6000$ K. As a consequence of the low space density of massive stars in high Galactic latitude fields, most MPMS stars targeted by the SDSS have temperatures $T_{\rm eff} \lesssim 8000$ K. In the overlap region between these two temperature ranges, the theoretical spectra confirm the expectation that MPMS stars have much narrower (i.e., smaller FWHM) Hα profiles than white dwarfs.

Figure 3 is representative of the relationship between Balmer line features as a function of $T_{\rm eff}$ and $\log g$. Above $T_{\rm eff} \approx 6000$ K, MPMS star and white dwarf spectra are visually differentiable on many 2D slices

[1] A Voigt profile is a convolution of Gaussian and Lorentzian profiles that well-approximates the pressure-broadened wings of the Balmer lines (e.g., Tremblay & Bergeron 2009).

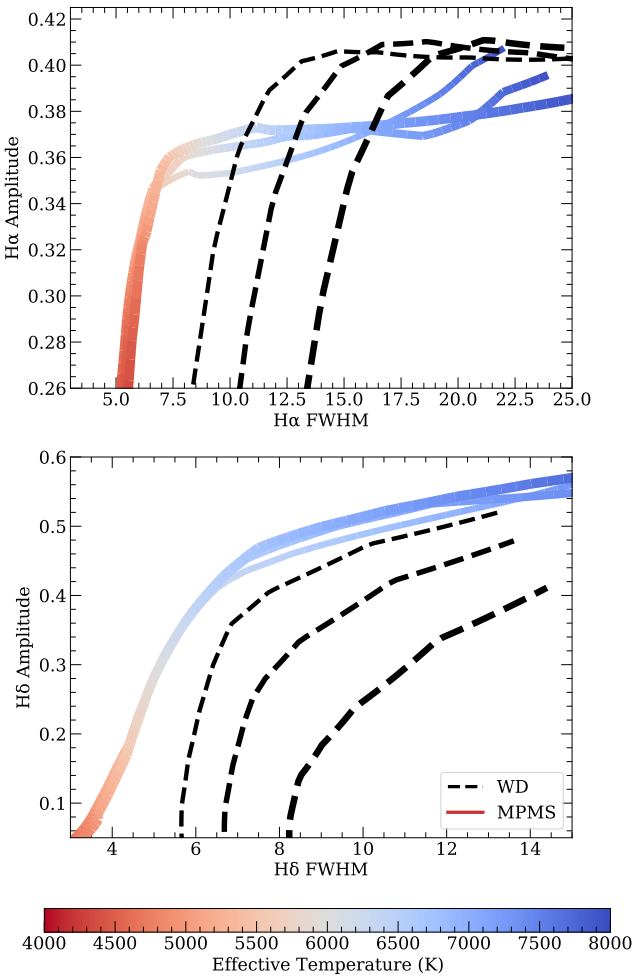

Figure 3. Two "slices" of the Balmer line phase space for MPMS stars (solid lines colored by effective temperature) and white dwarfs (dashed lines). The thickness of each line is proportional to surface gravity $\log g = 4$, 4.5, 5 for MPMS star models and $\log g = 7.5$, 8, 8.5 for white dwarf models.

through Balmer line phase space. Below $T_{\rm eff} \approx 6000$ K, the higher-order Balmer lines in white dwarf spectra start to rapidly lose their intensities. In the range $5000 \text{ K} \lesssim T_{\rm eff} \lesssim 6000$ K, combining statistics from several Balmer lines can still separate MPMS stars from white dwarfs. Below $T_{\rm eff} \approx 5000$ K, the Balmer lines for both metal-free low-mass stars and white dwarfs begin to disappear altogether, resulting in pure-continuum spectra (Blouin et al. 2019). In other words, below $T_{\rm eff} \approx 5000$ K there is no way to use optical spectra to distinguish low-mass Population III stars from white dwarfs. We discuss this special case of very low-mass Population III stars further in Section 4.

3.2. *Synthetic Photometry*

In addition to the Balmer features we extract from each theoretical spectrum, we also calculate synthetic

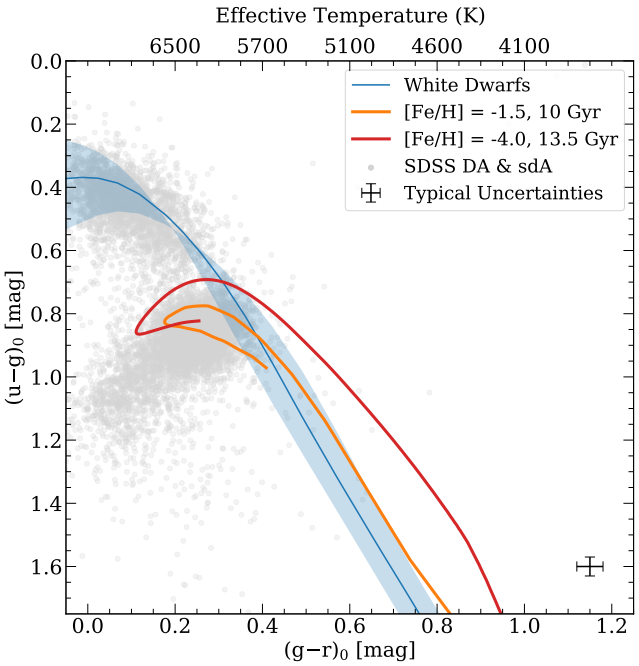

Figure 4. Synthetic color–color diagram using SDSS bands. The blue line corresponds to white dwarfs with $\log g = 8$ while the shaded region indicates the locus of white dwarfs with surface gravities in the range $7 < \log g < 9$. We also plot MIST isochrones for MPMS stars with [Fe/H] $= -1.5$ and age 10 Gyr (orange) and [Fe/H] $= -4.0$ and age 13.5 Gyr (red). We overlay as gray points all stars classified as "DA", "sdA", or "sdA/F" objects by Kepler et al. (2019).

photometry in several photometric systems using the `pyphot` utility (Fouesneau 2020). We calculate synthetic absolute magnitudes in the SDSS *ugriz*, Pan-STARRS *grizy* (Chambers et al. 2016), SkyMapper *uvgriz* (Bessell et al. 2011), DECam *ugrizY* (Flaugher et al. 2015), and Vera Rubin Observatory *ugrizy* (Ivezic et al. 2019) systems. While the software accompanying this paper can be used with any of these photometric systems, we focus on SDSS photometry colors in this paper since we validate our method on SDSS data.

We plot in Figure 4 a comparison between MPMS stars and white dwarfs in Sloan color–color space. Sloan $u-g$ color is strongly affected by the Balmer jump, a sensitive probe of surface gravity. A $u-g$ versus $g-r$ color–color plot can therefore be used to cleanly differentiate relatively warm MPMS stars and white dwarfs. At lower temperatures the difference becomes less pronounced, so this color–color diagram can only differentiate MPMS stars and white dwarfs when $T_{\rm eff} \gtrsim 6000$. While Figure 4 depicts one well known photometric difference between MPMS stars and white dwarfs, we consider the complete color–color spaces defined by each of the SDSS, Pan-STARRS, SkyMapper, DECam, and Rubin Observatory photometric systems, computing all unique pairwise differences of the magnitudes in each photometric band. While the approach that we describe in the following subsection is related to traditional color–color selections (e.g., Lokhorst et al. 2016; Pelisoli et al. 2018b), our approach uses the entire N-dimensional color space distribution at once rather than relying on individual 2D slices through that space.

3.3. *Logistic Regression Classifier*

To map the spectroscopic and photometric features described above to a MPMS star or white dwarf classification, we use a logistic regression classifier. A logistic regression is a model that assumes a linear relationship between the input features and the log-odds of a binary (i.e., Bernoulli) random variable taking on the value 1 (or "true"). Given input features $\mathbf{x} = [x_0, x_1, x_2, \ldots]$, fitting a logistic regression involves solving for the coefficients $\boldsymbol{\beta} = [\beta_0, \beta_1, \beta_2, \ldots]$ such that

$$\boldsymbol{\beta}^{\intercal}\mathbf{x} = \log\left(\frac{p}{1-p}\right), \tag{1}$$

where p is the probability that the Bernoulli random variable is 1 (or "true"). A logistic regression model is typically fit to data with known labels (i.e., where p is known to be either zero or one), and the coefficients $\boldsymbol{\beta}$ are subsequently used to estimate $\hat{p}$ for new input data. There is no closed-form solution to determine $\boldsymbol{\beta}$, so an iterative gradient descent algorithm is often used to find the optimal coefficients.

We define the underlying Bernoulli variable to have value 0 if an object is a confirmed white dwarf and 1 if an object is a confirmed metal-poor main-sequence star. The associated probability in the model can therefore be defined as $p = P_{\rm MPMS}$, the probability that a given object is a MPMS star as opposed to a white dwarf. We demonstrate three possible input configurations: the Balmer line summary statistics (eight features), *ugriz* photometric colors (ten features), and *griz* photometric colors (six features). We also consider a combined classifier that uses *ugriz* colors and Balmer features simultaneously.

We use a logistic regression model due to its simplicity and ease of interpretation. The classification probability $P_{\rm MPMS}$ returned by a logistic regression is well-calibrated by default (Yu et al. 2011), providing confidence in the classification. We found that using a more complex classification algorithm like a random forest or support vector machine increased the complexity of the method without much increase in accuracy. In addition, these other algorithms require an external "calibration function" to transform the returned classification prob-

abilities to statistically meaningful values (Niculescu-Mizil & Caruana 2005). This step is unnecessary for the logistic regression.

When training our logistic regression models, we reserve 5% of the stars in our grid of theoretical models as a synthetic validation set. We evaluate our logistic regression model on these unseen synthetic validation data and confirm that the model correctly predicts their classifications virtually 100% of the time. This validation step ensures that the logistic regression is working as expected on noiseless synthetic data. We will further validate our logistic regression model with SDSS photometry and spectroscopy for objects with secure parallax-based classifications in Section 3.4. Our classifier and synthetic training data for the SDSS, Pan-STARRS, SkyMapper, DECam, and Rubin Observatory photometric systems are publicly available.[2]

3.4. *Model Validation with Objects that have Secure Empirical Classifications*

We now further validate our classifier with the empirical validation sample of 1807 objects described in Section 2.2. These objects were classified by Kepler et al. (2019) based on spectroscopic features with Gaia DR2-confirmed classifications as either MPMS stars or white dwarfs. We confirm that the Kepler et al. (2019) classifications for these objects are accurate based on our inspection of their locations in a color–magnitude diagram. We use the available SDSS photometry and spectroscopy for this empirical validation sample to compute Balmer features and *ugriz* colors. We then run the logistic regression classifier described in Section 3.3 on these features to predict based solely on SDSS photometry and spectroscopy the probability that each object is a MPMS star.

Receiver operating characteristic (ROC) curves are one way to graphically evaluate classifiers. ROC curves describe the relationship between the true-positive and false-positive rates of a classifier as a function of its acceptance threshold (i.e., the output probability above which a "positive" classification is made). ROC curves provide a high-level summary of the sensitivity (i.e., probability of detection) and specificity (i.e., probability of false alarm). Precision-recall (PR) curves provide an alternative graphical classifier diagnostic. They are particularly useful for our application, as precision (i.e., the probability that a MPMS star is accurately classified by our classifier) is the most important metric for our scientific goal. PR curves are also more agnostic to the possible existence of class imbalance in a data set, as is the case in our empirical validation sample in which there are twice as many white dwarfs as MPMS stars. Together, ROC and PR curves provide an overview of the performance of a classifier.

We illustrate in Figure 5 ROC and PR curves for the application of our classifiers to our empirical validation data. We evaluate our logistic regression classifier in several scenarios: only the eight Balmer-line-summary-based features, only the ten *ugriz* colors, only the six *griz* colors, and both the Balmer-line-summary-based features and *ugriz* colors. As expected, the Balmer spectroscopic features provide the most discriminating power. The inclusion of $u-g$ color greatly improves the quality of classifications compared to *griz* colors alone, as $u-g$ color is sensitive to $\log g$ via the Balmer break.

In terms of precision, the classifier using both photometric and spectroscopic features far outperforms the spectroscopy-only classifier. This implies that a degeneracy in spectroscopic features in MPMS star and white dwarf spectra can be overcome by including photometric features. That natural interpretation is that the photometric colors provide a strong constraint on temperature, breaking the $T_{\rm eff}$–$\log g$ degeneracy of the absorption line features. We validate the naive expectation that classifiers using more than one Balmer line are superior to any classifier based on a single line. We find that classification performance is most enhanced when lower-order Balmer lines like Hα are combined with higher-order lines like Hδ and confirm that the best performance is achieved when all four Balmer lines are included. We conclude that our combined photometric and spectroscopic classifier has the accuracy and precision necessary to separate MPMS stars from white dwarfs using SDSS data or equivalent LAMOST or DESI data.

While our photometry-only classifier can be used to separate MPMS stars from white dwarfs, it is susceptible to many of the issues with traditional color–color selections. For example, the colors of white dwarfs with heavily metal-polluted photospheres will change due to line blanketing and changes in continuum opacity. While metal-polluted white dwarfs could be misclassified by our photometry-only classifier, they are easy to remove from a joint photometric/spectroscopic search for metal-poor stars due to their prominent metal absorption lines. Our classifier is therefore most powerful when spectroscopic data are available.

3.5. *Approximate Determination of Metallicity*

After differentiating MPMS stars from white dwarfs, another important task is to select the most metal-poor

[2] https://github.com/vedantchandra/mpms

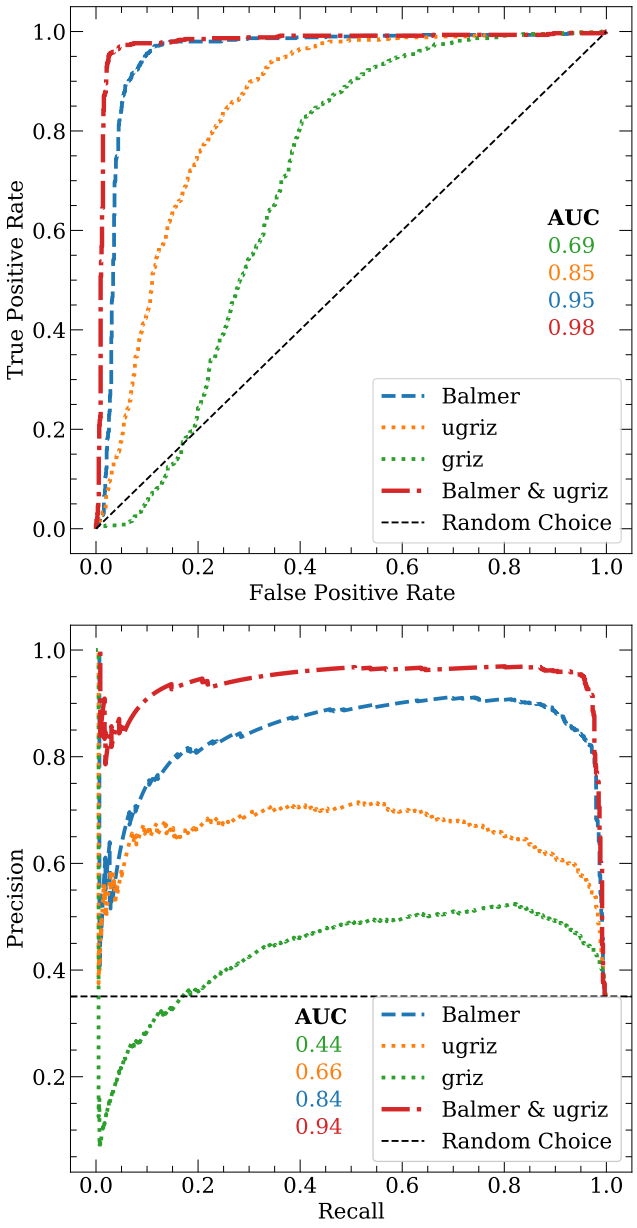

Figure 5. Receiver operating characteristic (ROC) and precision-recall (PR) curves for the photometry-only, spectroscopy-only, and combined logistic regression classifiers trained on theoretical models and validated with classifications confirmed by high-quality Gaia DR2 parallaxes. The classifier that uses both spectroscopic and photometric features achieves the best performance, followed closely by the classifier that uses only spectroscopic features. Classifiers that use only photometric features achieve acceptable performance but lag behind classifiers that utilize spectroscopic features.

candidates among the predicted MPMS stars. In order to select the most metal-poor MPMS star candidates, we implement a simple method to approximately quantify stellar metallicity from MPMS star spectra by fitting them with theoretical spectra.

We first use SDSS photometry and any available Gaia parallax information to generate an initial set of spectroscopic stellar parameters $T_{\rm eff}$, $\log g$, and [Fe/H]. We define a χ^2 statistic by comparing the observed SDSS *ugriz* photometry dereddened as described in Section 2.2 to MESA Isochrones & Stellar Tracks (MIST) *ugriz* photometry (Dotter 2016; Choi et al. 2016; Paxton et al. 2011, 2013, 2015, 2018). To account for the low-precision parallaxes available in most cases, we use an exponentially decreasing space density prior on parallax (Bailer-Jones 2015). We sample with `emcee` (Foreman-Mackey et al. 2013; Foreman-Mackey et al. 2019) the posterior distribution of the fundamental stellar parameters (e.g., mass, age, and metallicity) conditioned on the data, taking $-0.5 \cdot \chi^2$ as the log-likelihood of the data. We then identify the maximum-likelihood sample and interpolate the MIST isochrone grid to define an initial set of spectroscopic stellar parameters $T_{\rm eff}$, $\log g$, and [Fe/H].

Next, we fit PHOENIX theoretical spectra from Husser et al. (2013) spanning the range 3000 K $\leq T_{\rm eff} \leq$ 8000 K, $3.5 \leq \log g \leq 6.5$, and $-4 \leq$ [Fe/H] ≤ 0 to the observed SDSS MPMS star spectra using a a two-step fitting procedure. We initialize the stellar parameters at the photometrically-inferred values described above. We first fit the sky emission line at 4047 Å in each SDSS spectrum with a Gaussian to estimate the instrumental line-spread function. We then convolve the grid of theoretical spectra with this kernel to bring them to the instrumental resolution. We next fit a straight line to a region around Hα in each SDSS spectrum and then divide the flux by that line to approximately normalize the spectrum in the vicinity of the line. We then fit a Gaussian to Hα and use its known wavelength to correct each SDSS spectrum to the rest frame. To spectroscopically infer $T_{\rm eff}$ and $\log g$, we assume a fixed [Fe/H] $= -2$ and fit the grid of theoretical spectra to the continuum-normalized Balmer lines. To spectroscopically infer [Fe/H], we fix the $T_{\rm eff}$ and $\log g$ derived in the previous step and fit the continuum-normalized Ca II K absorption line to infer [Ca/H] and thereby [Fe/H] assuming [Ca/Fe] $= 0$. For each absorption line, we fit the theoretical spectra using a non-linear least squares algorithm `lmfit` (Newville et al. 2014) that minimizes the squared residual between the observed and theoretical spectra. We alternate the Balmer-based $T_{\rm eff}$ & $\log g$ and the Ca II K-based [Fe/H] inferences until the spectroscopic stellar parameters are self-consistent. In prac-

tice this only requires one or two iterations since the Balmer-based inference is quite independent of metallicity.

For the metal-poor main sequence stars with published spectroscopic stellar parameters from higher resolution or signal-to-noise ratio (S/N) data, we find that the spectroscopically derived parameters are better than those based on photometry and astrometry. This is likely due to the low-quality parallaxes available in most cases. Additionally, we note that spectroscopic Fe/H inferences based on the Ca II K absorption line can be overestimated if the star is carbon-enhanced, since the Ca II K line is blended with nearby carbon features on the mid-resolution spectra (e.g., Frebel et al. 2015). Since our primary goal is to find the most metal-poor candidates (including those depleted in carbon), we do not correct for this effect explicitly, but we caution that our spectroscopically-inferred metallicities should be treated as indicative estimates only.

4. RESULTS

With the accuracy and precision of our classifier now established, we can now classify the entire sample of 14,522 MPMS star/white dwarf candidates from Kepler et al. (2019) with SDSS photometry and spectroscopy. We fit the Balmer lines of these spectra to derive the line summaries described in Section 3.1. We then apply our combined logistic regression classifier to the Balmer features and *ugriz* colors of these stars. The result of this process is a prediction of the probability $P_{\rm MPMS}$ that a spectrum was produced by a MPMS star as opposed to a white dwarf. Reassuringly, the distribution of probabilities is bimodal: most stars have probabilities close to zero or one. This distribution provides even more confidence that our classifier is both precise and accurate. We decide on decision threshold of 0.5 and classify all objects with $P_{\rm MPMS} > 0.5$ as MPMS star candidates.

We find that approximately 95% of our logistic regression-based classifications agree with the visual inspection-based classifications reported in (Kepler et al. 2019). The 5% of cases where our classifier disagrees with Kepler et al. (2019) are due to objects with extremely low S/N spectra. Spectroscopic surveys like DESI will produce hundreds of thousands of spectra plausibly produced by MPMS stars or white dwarfs, and only our automated classification approach will be able to scale to that data volume.

We emulate future searches for candidate extremely metal-poor (EMP) stars in upcoming surveys like SDSS-V and DESI by mining the stars in our SDSS data set for EMP candidates. Numerous studies have already searched these SDSS data for metal-poor stars (e.g., Allende Prieto et al. 2006, 2008, 2014, 2015; Caffau et al. 2011a,b; Bonifacio et al. 2012, 2015; Aoki et al. 2013; Frebel et al. 2015; Placco et al. 2015; Aguado et al. 2016, 2017a,b, 2018a,b; Yoon et al. 2016; Carbon et al. 2017), so our expectation is that many of the most promising candidates have already been discovered. We select all stars from the 12,000 star subsample of the Kepler et al. (2019) study referenced above with $P_{\rm MPMS} > 0.5$ according to our combined classifier as possible MPMS candidates. This leaves us with 10,500 MPMS star spectra for which we compute approximate metallicities as described in Section 3.5. We selected stars with the lowest estimated metallicities and visually inspected their spectra, examining the Ca II K (3934.8 Å), Na I (5895.6 Å), and Mg I (5176.7 Å) lines in particular. We report our most promising candidates in Table 1, along with our spectroscopically-inferred estimates of $T_{\rm eff}$, $\log g$, and [Fe/H].

In addition, we use SIMBAD to search for literature references to our candidate MPMS stars (Wenger et al. 2000). While several of our MPMS star candidates have no prior reference in the literature, we find that our selection turns up dozens of previously-known metal-poor stars with confirmed metallicities [Fe/H] < -3.0. A selection of these stars is included in Table 1. We therefore conclude that SDSS data have already been exhaustively searched for extremely metal-poor stars. Nevertheless, this serves as a comprehensive validation of our methodology to search for metal-poor stars in future spectroscopic surveys.

While the existence of low-mass Population III stars is still debated, we assert that it will be possible to uniquely classify a featureless optical spectrum plausibly produced be either a low-mass Population III star or a cool white dwarf based on the optical-to-infrared colors of the object. The lowest mass primordial-composition object that can burn hydrogen should have $M_* \approx 0.1\ M_\odot$. Stellar models therefore predict a lower limit on the effective temperature of Population III stars of $T_{\rm eff} \approx 3600$ K (Burrows et al. 1993; Saumon et al. 1994). At these temperatures, the optical spectra of the coolest primordial stars will be indistinguishable from the optical spectra of white dwarfs because both will have pure-continuum spectra with no Balmer or metal lines.

However, collision-induced absorption (CIA) from molecular hydrogen will produce surface gravity-dependent continuum features in the red optical and infrared (Saumon et al. 1994; Blouin et al. 2017, 2019). At a given temperature (or $g - r$ color), a white dwarf will have more CIA than a low-mass Population III star due to its higher surface gravity. White dwarfs will con-

Table 1. Extremely Metal-poor Candidates Identified in This Study

Gaia DR2 Source ID	R.A. (deg)	Decl. (deg)	Sloan Plate-MJD-Fiber	g (mag)	$T_{\rm eff}$ (K)	$\log g$	[Fe/H]	Reference
3724067121891339648	211.826	10.505	1703-53799-0013	16.9	6441	4.0	-4.0	
874891332185786752	116.953	26.762	2055-53729-0121	17.3	6450	3.7	-4.0	
4465215302785008640	245.076	16.141	2188-54595-0026	18.5	6550	4.1	-3.9	
1448863790892447744	203.103	27.516	2245-54208-0450	16.8	6435	4.0	-3.8	
3958825597588943232	189.109	23.019	3374-54948-0220	18.2	6453	3.7	-3.8	
3905214200892445184	184.325	8.870	5396-55947-0370	19.4	6560	4.5	-3.8	
1493736818927192576	220.706	44.954	6046-56096-0550	18.8	6359	4.0	-3.8	
3092216989574463616	126.339	4.059	1185-52642-0519	17.1	6441	4.0	-3.9	Aoki et al. (2013)
290930261314166528	25.151	23.749	2044-53327-0515	15.8	6354	4.8	-3.5	Arentsen et al. (2019)
1276882477044162688	230.509	30.924	1651-53442-0330	16.6	6333	4.7	-3.4	Aoki et al. (2013)
4190837398756490112	301.306	-10.751	2303-54629-0377	17.0	6536	3.8	-3.6	François et al. (2018)
1184737183522291712	221.669	12.822	1712-53531-0636	16.2	6445	4.0	-2.9	Aoki et al. (2013)
3740963179636227968	207.345	14.127	1777-53857-0479	16.6	6340	3.8	-3.5	Bonifacio et al. (2018)
3976087728282022272	175.848	20.349	2506-54179-0576	16.9	6426	4.0	-2.9	Yoon et al. (2016)
3890626773968983296	157.313	17.491	2853-54440-0113	16.9	6047	4.7	-4.0	Caffau et al. (2011a)
1609914447333432192	213.030	56.159	2447-54498-0274	16.0	6488	3.8	-4.0	Aoki et al. (2013)
1195572458297534080	233.443	15.950	2782-54592-0411	16.9	6562	4.0	-4.0	Caffau et al. (2013)
931227322991970560	123.976	47.496	3693-55208-0408	17.1	6523	4.6	-4.0	Aguado et al. (2018b)
2548541852945056896	5.808	3.133	4299-55827-0002	17.9	6404	4.0	-4.0	Aguado et al. (2018a)

NOTE—We indicate SIMBAD references for stars with confirmed [Fe/H] < -3.0 inferences. $T_{\rm eff}$, $\log g$ and [Fe/H] are estimated from Sloan spectra with the spectroscopic fitting routine described in Section 3.5.

sequently be fainter than low-mass Population III stars in the red optical izy and infrared bands like JHK. Therefore, at constant temperature photometric colors comparing optical to red optical or infrared bands (e.g., $r-z$, $V-J$, etc.) will be bluer for white dwarfs than low-mass Population III stars. This effect is expected to be larger than the typical photometric uncertainties in ground-based surveys like the SDSS, Pan-STARRS, SkyMapper, or DES (Saumon et al. 1994; Blouin et al. 2017).

While future work on CIA opacities will enable a more quantitative comparison, current uncertainties in the theoretical modeling of CIA make it challenging to precisely quantify the expected difference between low-mass Population III stars and white dwarfs, and thereby build a predictive model like the one we presented for warmer stars. Nevertheless, we predict that the photometric signature of CIA should be detectable via infrared photometry and consequently able to differentiate between low-mass Population III stars and white dwarfs even without parallax information.

5. DISCUSSION

We have developed a classification framework that can be used to differentiate low-mass Population III stars from white dwarfs in future spectroscopic surveys. Since our techniques primarily rely on Balmer lines and broad-band photometry, our methods naturally extend to the identification of metal-poor stars including the sought-after EMP and ultra metal-poor (UMP) stars (i.e., stars with [Fe/H] $\lesssim -4$). Another natural application of our technique is the identification and removal of the subdwarf stars that frequently contaminate catalogs of white dwarf candidates (Kepler et al. 2019).

The typical white dwarf has $M_* \approx 0.6\ M_\odot$, $R_* \approx R_\oplus$, and consequently $\log g \sim 8$. Its surface gravity is therefore orders of magnitude larger than the typical metal-poor main sequence star surface gravity $\log g \lesssim 5$. As a result, our classifier gains most of its discriminatory power from an object's surface gravity. While MPMS stars are well separated from typical white dwarfs in $\log g$, MPMS stars can overlap in $\log g$ with ELM white dwarfs produced by mass transfer in multiple systems (e.g., Brown et al. 2010; Pelisoli et al. 2017; Pelisoli & Vos 2019; Pelisoli et al. 2019). Because of their lower

masses and larger radii than typical white dwarfs, ELM white dwarfs can have lower $\log g$ and much narrower Balmer lines than typical white dwarfs. Their narrow Balmer lines could cause our classifier to misidentify them as MPMS stars. While the identification of these relatively rare ELM white dwarfs is a worthwhile goal in its own right, it is not the main objective of our current analysis. We argue that in future searches for MPMS or low-mass Population III stars, ELM white dwarfs can be filtered out by directly fitting theoretical spectra to Balmer lines to infer $\log g$. Indeed, even the least-massive ELM white dwarfs should have $\log g \gtrsim 5$ while MPMS stars with $M_* \gtrsim 0.1\ M_\odot$ will have $\log g \lesssim 5$ (Brown et al. 2010; Dotter 2016; Choi et al. 2016).

It remains an open question whether or not low-mass Population III stars exist in the local Universe. Beyond awaiting serendipitous direct detections, Galactic/stellar archaeology provide a promising technique to probe the hypothesis of surviving Population III stars and to constrain the primordial initial mass function. Hartwig et al. (2015) proposed that a total sample size of order 10^7 halo stars is required to rule out Population III survivors at the 95% confidence level. However, this is likely an overestimate since it only considers blind surveys. In practice, searching for EMP and UMP stars is far more efficient. Magg et al. (2019) suggested instead to use the occurrence of EMP and UMP stars to constrain the existence of Population III survivors. The largest uncertainty in this method by far is the total number of EMP and UMP stars in the Milky Way's stellar halo. As a result, a comprehensive search for such stars is an important need.

6. CONCLUSION

While it is trivial to separate metal-poor main sequence stars and white dwarfs when high-quality parallaxes are available, even post-Gaia many objects with DESI or Sloan spectroscopy will lack reliable parallaxes. For that reason, we developed a classifier capable of separating metal-poor main sequence stars from cool white dwarfs using a range of photometric and spectroscopic features. We trained and validated our classifier using theoretical spectra and synthetic photometry. We also validated the classifier using objects securely classified as metal-poor main sequence stars or white dwarfs based on Sloan spectroscopy and high-quality Gaia DR2 parallaxes. We then applied our classifier to a sample of candidate metal-poor main sequence stars and white dwarfs with visual classifications and confirmed that our automated approach reproduces the human classifications. We make our classifier and its underlying source code publicly available[2] for reproducibility and application to future survey data. For the stars classified as metal-poor main sequence stars, we executed a search for extremely metal-poor stars. We uncovered some previously unidentified candidates and flagged dozens of already confirmed extremely metal-poor stars. We predict that the application of our classifier to future DESI and SDSS-V spectroscopy will discover thousands of metal-poor main sequence stars. We further predict that even in the absence of high-quality parallaxes, any candidate low-mass Population III stars identified by their featureless optical spectra can be separated from cool white dwarfs due to their redder optical-to-infrared colors. These red colors are produced by relatively weak collision-induced absorption from molecular hydrogen in the relatively low-surface gravity photospheres of low-mass Population III stars. The methods presented in this work will facilitate the rapid and reliable identification of MPMS stars, providing improved constraints on the uncertain existence of surviving pristine stars from the primordial Universe.

ACKNOWLEDGMENTS

We thank the anonymous referee for discerning suggestions that significantly improved both our analysis and this paper. We are grateful to Simon Blouin for providing his latest grid of theoretical cool white dwarf spectra as well as insightful comments and suggestions. We thank JJ Hermes, Vinicius Placco, Pier-Emmanuel Tremblay, Tilman Hartwig, Ingrid Pelisoli, and Davide Aguado for constructive conversations that significantly improved this paper. This material is based upon work supported by the Johns Hopkins University the Institute for Data Intensive Engineering & Science (IDIES).

This research has made use of the SIMBAD database (Wenger et al. 2000), operated at CDS, Strasbourg, France. This research has made use of NASA's Astrophysics Data System (ADS). Funding for the SDSS and SDSS-II has been provided by the Alfred P. Sloan Foundation, the Participating Institutions, the National Science Foundation, the U.S. Department of Energy, the National Aeronautics and Space Administration, the Japanese Monbukagakusho, the Max Planck Society, and the Higher Education Funding Council for England. The SDSS Web Site is http://www.sdss.org/. The SDSS is managed by the Astrophysical Research Consortium for the Participating Institutions. The Participating Institutions are the American Museum of Natural History, Astrophysical Institute Potsdam, University of Basel, University of Cambridge, Case Western Reserve University, University of Chicago, Drexel University, Fermilab, the Institute for Advanced Study,

the Japan Participation Group, Johns Hopkins University, the Joint Institute for Nuclear Astrophysics, the Kavli Institute for Particle Astrophysics and Cosmology, the Korean Scientist Group, the Chinese Academy of Sciences (LAMOST), Los Alamos National Laboratory, the Max-Planck-Institut für Astronomie (MPIA Heidelberg), the Max-Planck-Institut für Astrophysik (MPA Garching), New Mexico State University, Ohio State University, University of Pittsburgh, University of Portsmouth, Princeton University, the United States Naval Observatory, and the University of Washington. Funding for SDSS-III has been provided by the Alfred P. Sloan Foundation, the Participating Institutions, the National Science Foundation, and the U.S. Department of Energy Office of Science. The SDSS-III web site is http://www.sdss3.org/. SDSS-III is managed by the Astrophysical Research Consortium for the Participating Institutions of the SDSS-III Collaboration including the University of Arizona, the Brazilian Participation Group, Brookhaven National Laboratory, Carnegie Mellon University, University of Florida, the French Participation Group, the German Participation Group, Harvard University, the Instituto de Astrofísica de Canarias, the Michigan State/Notre Dame/JINA Participation Group, Johns Hopkins University, Lawrence Berkeley National Laboratory, Max-Planck-Institut für Astrophysik (MPA Garching), Max-Planck-Institut für Extraterrestrische Physik (MPE), New Mexico State University, New York University, Ohio State University, Pennsylvania State University, University of Portsmouth, Princeton University, the Spanish Participation Group, University of Tokyo, University of Utah, Vanderbilt University, University of Virginia, University of Washington, and Yale University. Funding for the Sloan Digital Sky Survey IV has been provided by the Alfred P. Sloan Foundation, the U.S. Department of Energy Office of Science, and the Participating Institutions. SDSS-IV acknowledges support and resources from the Center for High Performance Computing at the University of Utah. The SDSS website is www.sdss.org. SDSS-IV is managed by the Astrophysical Research Consortium for the Participating Institutions of the SDSS Collaboration including the Brazilian Participation Group, the Carnegie Institution for Science, Carnegie Mellon University, Center for Astrophysics — Harvard & Smithsonian, the Chilean Participation Group, the French Participation Group, Instituto de Astrofísica de Canarias, Johns Hopkins University, Kavli Institute for the Physics and Mathematics of the Universe (IPMU) / University of Tokyo, the Korean Participation Group, Lawrence Berkeley National Laboratory, Leibniz Institut für Astrophysik Potsdam (AIP), Max-Planck-Institut für Astronomie (MPIA Heidelberg), Max-Planck-Institut für Astrophysik (MPA Garching), Max-Planck-Institut für Extraterrestrische Physik (MPE), National Astronomical Observatories of China, New Mexico State University, New York University, University of Notre Dame, Observatário Nacional / MCTI, The Ohio State University, Pennsylvania State University, Shanghai Astronomical Observatory, United Kingdom Participation Group, Universidad Nacional Autónoma de México, University of Arizona, University of Colorado Boulder, University of Oxford, University of Portsmouth, University of Utah, University of Virginia, University of Washington, University of Wisconsin, Vanderbilt University, and Yale University. This work has made use of data from the European Space Agency (ESA) mission Gaia (https://www.cosmos.esa.int/gaia), processed by the Gaia Data Processing and Analysis Consortium (DPAC, https://www.cosmos.esa.int/web/gaia/dpac/consortium). Funding for the DPAC has been provided by national institutions, in particular the institutions participating in the Gaia Multilateral Agreement.

Facilities: Gaia, Sloan

Software: `numpy` (Harris et al. 2020), `scipy` (Virtanen et al. 2020), `matplotlib` (Hunter 2007), `astropy` (Robitaille et al. 2013), `scikit-learn` (Pedregosa et al. 2011), `lmfit` (Newville et al. 2014), `mwdust` (Bovy et al. 2016)

REFERENCES

Abel, T., Bryan, G. L., & Norman, M. L. 2000, ApJ, 540, 39, doi: 10.1086/309295

—. 2002, Science, 295, 93, doi: 10.1126/science.295.5552.93

Aguado, D. S., Allende Prieto, C., González Hernández, J. I., et al. 2016, A&A, 593, A10, doi: 10.1051/0004-6361/201628371

Aguado, D. S., Allende Prieto, C., González Hernández, J. I., & Rebolo, R. 2018a, ApJL, 854, L34, doi: 10.3847/2041-8213/aaadb8

Aguado, D. S., Allende Prieto, C., González Hernández, J. I., Rebolo, R., & Caffau, E. 2017a, A&A, 604, A9, doi: 10.1051/0004-6361/201731320

Aguado, D. S., González Hernández, J. I., Allende Prieto, C., & Rebolo, R. 2017b, A&A, 605, A40, doi: 10.1051/0004-6361/201730654

—. 2018b, ApJL, 852, L20, doi: 10.3847/2041-8213/aaa23a

Ahumada, R., Prieto, C. A., Almeida, A., et al. 2020, The Astrophysical Journal Supplement Series, 249, 3, doi: 10.3847/1538-4365/ab929e

Allende Prieto, C., Beers, T. C., Wilhelm, R., et al. 2006, ApJ, 636, 804, doi: 10.1086/498131

Allende Prieto, C., Sivarani, T., Beers, T. C., et al. 2008, AJ, 136, 2070, doi: 10.1088/0004-6256/136/5/2070

Allende Prieto, C., Fernández-Alvar, E., Schlesinger, K. J., et al. 2014, A&A, 568, A7, doi: 10.1051/0004-6361/201424053

Allende Prieto, C., Fernández-Alvar, E., Aguado, D. S., et al. 2015, A&A, 579, A98, doi: 10.1051/0004-6361/201525904

Aoki, W., Beers, T. C., Lee, Y. S., et al. 2013, Astronomical Journal, 145, doi: 10.1088/0004-6256/145/1/13

Arenou, F., Luri, X., Babusiaux, C., et al. 2018, A&A, 616, A17, doi: 10.1051/0004-6361/201833234

Arentsen, A., Starkenburg, E., Shetrone, M. D., et al. 2019, A&A, 621, A108, doi: 10.1051/0004-6361/201834146

Bailer-Jones, C. A. L. 2015, PASP, 127, 994, doi: 10.1086/683116

Beers, T. C., & Christlieb, N. 2005, ARA&A, 43, 531, doi: 10.1146/annurev.astro.42.053102.134057

Bessell, M., Bloxham, G., Schmidt, B., et al. 2011, PASP, 123, 789, doi: 10.1086/660849

Blanton, M. R., Bershady, M. A., Abolfathi, B., et al. 2017, The Astronomical Journal, 154, 28, doi: 10.3847/1538-3881/aa7567

Blouin, S., Dufour, P., & Allard, N. F. 2018a, The Astrophysical Journal, 863, 184, doi: 10.3847/1538-4357/aad4a9

Blouin, S., Dufour, P., Allard, N. F., & Kilic, M. 2018b, The Astrophysical Journal, 867, 161, doi: 10.3847/1538-4357/aae53a

Blouin, S., Dufour, P., Thibeault, C., & Allard, N. F. 2019, The Astrophysical Journal, 878, 63, doi: 10.3847/1538-4357/ab1f82

Blouin, S., Kowalski, P. M., & Dufour, P. 2017, The Astrophysical Journal, 848, 36, doi: 10.3847/1538-4357/aa8ad6

Bonifacio, P., Sbordone, L., Caffau, E., et al. 2012, Astronomy and Astrophysics, 542, 1, doi: 10.1051/0004-6361/201219004

Bonifacio, P., Caffau, E., Spite, M., et al. 2015, A&A, 579, A28, doi: 10.1051/0004-6361/201425266

—. 2018, A&A, 612, A65, doi: 10.1051/0004-6361/201732320

Bovy, J., Rix, H.-w., Green, G. M., Schlafly, E. F., & Finkbeiner, D. P. 2016, The Astrophysical Journal, 818, 130, doi: 10.3847/0004-637x/818/2/130

Bressan, A., Marigo, P., Girardi, L., et al. 2012, Monthly Notices of the Royal Astronomical Society, 427, 127, doi: 10.1111/j.1365-2966.2012.21948.x

Bromm, V. 2013, Reports on Progress in Physics, 76, 112901, doi: 10.1088/0034-4885/76/11/112901

Bromm, V., Coppi, P. S., & Larson, R. B. 1999, ApJL, 527, L5, doi: 10.1086/312385

—. 2002, ApJ, 564, 23, doi: 10.1086/323947

Brown, T. M., Sahu, K., Anderson, J., et al. 2010, Astrophysical Journal Letters, 725, 19, doi: 10.1088/2041-8205/725/1/L19

Brown, W. R., Kilic, M., & Gianninas, A. 2017, The Astrophysical Journal, 839, 23, doi: 10.3847/1538-4357/aa67e4

Burrows, A., Hubbard, W. B., Saumon, D., & Lunine, J. I. 1993, ApJ, 406, 158, doi: 10.1086/172427

Caffau, E., Bonifacio, P., François, P., et al. 2011a, Nature, 477, 67, doi: 10.1038/nature10377

—. 2011b, A&A, 534, A4, doi: 10.1051/0004-6361/201117530

—. 2013, A&A, 560, A15, doi: 10.1051/0004-6361/201322213

Carbon, D. F., Henze, C., & Nelson, B. C. 2017, ApJS, 228, 19, doi: 10.3847/1538-4365/228/2/19

Chambers, K. C., Magnier, E. A., Metcalfe, N., et al. 2016, arXiv e-prints, arXiv:1612.05560. https://arxiv.org/abs/1612.05560

Chen, Y., Bressan, A., Girardi, L., et al. 2015, MNRAS, 452, 1068, doi: 10.1093/mnras/stv1281

Chen, Y., Girardi, L., Bressan, A., et al. 2014, MNRAS, 444, 2525, doi: 10.1093/mnras/stu1605

Choi, J., Dotter, A., Conroy, C., et al. 2016, ApJ, 823, 102, doi: 10.3847/0004-637X/823/2/102

Clark, P. C., Glover, S. C. O., Klessen, R. S., & Bromm, V. 2011a, ApJ, 727, 110, doi: 10.1088/0004-637X/727/2/110

Clark, P. C., Glover, S. C. O., Smith, R. J., et al. 2011b, Science, 331, 1040, doi: 10.1126/science.1198027

Cohen, J. G., Christlieb, N., Thompson, I., et al. 2013, ApJ, 778, 56, doi: 10.1088/0004-637X/778/1/56

Cui, X.-Q., Zhao, Y.-H., Chu, Y.-Q., et al. 2012, Research in Astronomy and Astrophysics, 12, 1197, doi: 10.1088/1674-4527/12/9/003

Dalton, G., Trager, S. C., Abrams, D. C., et al. 2012, in Society of Photo-Optical Instrumentation Engineers (SPIE) Conference Series, Vol. 8446, Ground-based and Airborne Instrumentation for Astronomy IV, 84460P, doi: 10.1117/12.925950

Dawson, K. S., Schlegel, D. J., Ahn, C. P., et al. 2013, AJ, 145, 10, doi: 10.1088/0004-6256/145/1/10

Dawson, K. S., Kneib, J.-P., Percival, W. J., et al. 2016, AJ, 151, 44, doi: 10.3847/0004-6256/151/2/44

DESI Collaboration, Aghamousa, A., Aguilar, J., et al. 2016, arXiv e-prints, arXiv:1611.00036. https://arxiv.org/abs/1611.00036

Doi, M., Tanaka, M., Fukugita, M., et al. 2010, AJ, 139, 1628, doi: 10.1088/0004-6256/139/4/1628

Dopcke, G., Glover, S. C. O., Clark, P. C., & Klessen, R. S. 2013, ApJ, 766, 103, doi: 10.1088/0004-637X/766/2/103

Dotter, A. 2016, ApJS, 222, 8, doi: 10.3847/0067-0049/222/1/8

Drimmel, R., Cabrera-Lavers, A., & López-Corredoira, M. 2003, Astronomy and Astrophysics, 409, 205, doi: 10.1051/0004-6361:20031070

Eisenstein, D. J., Weinberg, D. H., Agol, E., et al. 2011, AJ, 142, 72, doi: 10.1088/0004-6256/142/3/72

Flaugher, B., Diehl, H. T., Honscheid, K., et al. 2015, Astronomical Journal, doi: 10.1088/0004-6256/150/5/150

Foreman-Mackey, D., Hogg, D. W., Lang, D., & Goodman, J. 2013, Publications of the Astronomical Society of the Pacific, doi: 10.1086/670067

Foreman-Mackey, D., Farr, W., Sinha, M., et al. 2019, JOSS, 4, 1864, doi: 10.21105/joss.01864

Fouesneau, M. 2020, pyphot – A tool for computing photometry from spectra, GitHub. https://github.com/mfouesneau/pyphot

François, P., Caffau, E., Bonifacio, P., et al. 2018, A&A, 620, A187, doi: 10.1051/0004-6361/201834375

Fraser, M., Casey, A. R., Gilmore, G., Heger, A., & Chan, C. 2017, MNRAS, 468, 418, doi: 10.1093/mnras/stx480

Frebel, A., Chiti, A., Ji, A. P., Jacobson, H. R., & Placco, V. M. 2015, Astrophysical Journal Letters, 810, L27, doi: 10.1088/2041-8205/810/2/L27

Frebel, A., Chiti, A., Ji, A. P., Jacobson, H. R., & Placco, V. M. 2015, ApJL, 810, L27, doi: 10.1088/2041-8205/810/2/L27

Frebel, A., & Norris, J. E. 2015, ARA&A, 53, 631, doi: 10.1146/annurev-astro-082214-122423

Fukugita, M., Ichikawa, T., Gunn, J. E., et al. 1996, AJ, 111, 1748, doi: 10.1086/117915

Gaia Collaboration, Prusti, T., de Bruijne, J. H. J., et al. 2016, A&A, 595, A1, doi: 10.1051/0004-6361/201629272

Gaia Collaboration, Brown, A. G. A., Vallenari, A., et al. 2018, A&A, 616, A1, doi: 10.1051/0004-6361/201833051

Gänsicke, B. T., Koester, D., Farihi, J., et al. 2012, MNRAS, 424, 333, doi: 10.1111/j.1365-2966.2012.21201.x

Glover, S. 2013, Astrophysics and Space Science Library, Vol. 396, The First Stars (Springer), 103, doi: 10.1007/978-3-642-32362-1_3

Green, G. M., Schla, E., Zucker, C., Speagle, J. S., & Finkbeiner, D. 2019, ApJ, 93, doi: 10.3847/1538-4357/ab5362

Greif, T. H. 2015, Computational Astrophysics and Cosmology, 2, 3, doi: 10.1186/s40668-014-0006-2

Greif, T. H., Bromm, V., Clark, P. C., et al. 2012, MNRAS, 424, 399, doi: 10.1111/j.1365-2966.2012.21212.x

Greif, T. H., Springel, V., White, S. D. M., et al. 2011, ApJ, 737, 75, doi: 10.1088/0004-637X/737/2/75

Gunn, J. E., Carr, M., Rockosi, C., et al. 1998, AJ, 116, 3040, doi: 10.1086/300645

Gunn, J. E., Siegmund, W. A., Mannery, E. J., et al. 2006, AJ, 131, 2332, doi: 10.1086/500975

Hansen, C. J., Koch, A., Mashonkina, L., et al. 2020, Astronomy & Astrophysics. https://arxiv.org/abs/2009.11876

Harris, C. R., Millman, K. J., van der Walt, S. J., et al. 2020, Nature, 585, 357, doi: 10.1038/s41586-020-2649-2

Hartwig, T., Bromm, V., Klessen, R. S., & Glover, S. C. 2015, Monthly Notices of the Royal Astronomical Society, 447, 3892, doi: 10.1093/mnras/stu2740

Hirano, S., & Bromm, V. 2017, MNRAS, 470, 898, doi: 10.1093/mnras/stx1220

Hunter, J. D. 2007, Computing in Science and Engineering, 9, 90, doi: 10.1109/MCSE.2007.55

Husser, T. O., Wende-Von Berg, S., Dreizler, S., et al. 2013, Astronomy and Astrophysics, 553, 1, doi: 10.1051/0004-6361/201219058

Ishigaki, M. N., Tominaga, N., Kobayashi, C., & Nomoto, K. 2018, ApJ, 857, 46, doi: 10.3847/1538-4357/aab3de

Ivezic, Z., Kahn, S. M., Tyson, J. A., et al. 2019, The Astrophysical Journal, 873, 111, doi: 10.3847/1538-4357/ab042c

Kepler, S. O., Pelisoli, I., Koester, D., et al. 2019, Monthly Notices of the Royal Astronomical Society, 486, 2169, doi: 10.1093/mnras/stz960

Kobayashi, C., Karakas, A. I., & Lugaro, M. 2020, ApJ, 900, 179, doi: 10.3847/1538-4357/abae65

Koester, D., Gänsicke, B. T., & Farihi, J. 2014, Astronomy and Astrophysics, 566, doi: 10.1051/0004-6361/201423691

Kollmeier, J. A., Zasowski, G., Rix, H.-W., et al. 2017, in Bulletin of the American Astronomical Society, 274. https://arxiv.org/abs/1711.03234

Kosakowski, A., Kilic, M., Brown, W. R., & Gianninas, A. 2020, The Astrophysical Journal, 894, 53, doi: 10.3847/1538-4357/ab8300

Kroupa, P. 2001, Monthly Notices of the Royal Astronomical Society, 322, 231, doi: 10.1046/j.1365-8711.2001.04022.x

—. 2002, Science, 295, 82, doi: 10.1126/science.1067524

Lindegren, L., Hernández, J., Bombrun, A., et al. 2018, Astronomy and Astrophysics, 616, doi: 10.1051/0004-6361/201832727

Lokhorst, D., Starkenburg, E., McConnachie, A. W., et al. 2016, ApJ, 819, 124, doi: 10.3847/0004-637X/819/2/124

Luri, X., Brown, A. G., Sarro, L. M., et al. 2018, Astronomy and Astrophysics, 616, A9, doi: 10.1051/0004-6361/201832964

Luyten, W. J. 1922, LicOB, 336, 135

Magg, M., Klessen, R. S., Glover, S. C., & Li, H. 2019, Monthly Notices of the Royal Astronomical Society, 487, 486, doi: 10.1093/mnras/stz1210

Marrese, P. M., Marinoni, S., Fabrizio, M., & Altavilla, G. 2019, A&A, 621, A144, doi: 10.1051/0004-6361/201834142

Marshall, D. J., Robin, A. C., Reylé, C., Schultheis, M., & Picaud, S. 2006, Astronomy & Astrophysics, 651, 635

Newville, M., Ingargiola, A., Stensitzki, T., & Allen, D. B. 2014, Zenodo, , doi: 10.5281/ZENODO.11813

Niculescu-Mizil, A., & Caruana, R. 2005, in Proceedings of the 22nd International Conference on Machine Learning, ICML '05 (New York, NY, USA: Association for Computing Machinery), 625–632, doi: 10.1145/1102351.1102430

Padmanabhan, N., Schlegel, D. J., Finkbeiner, D. P., et al. 2008, ApJ, 674, 1217, doi: 10.1086/524677

Paxton, B., Bildsten, L., Dotter, A., et al. 2011, ApJS, 192, 3, doi: 10.1088/0067-0049/192/1/3

Paxton, B., Cantiello, M., Arras, P., et al. 2013, ApJS, 208, 4, doi: 10.1088/0067-0049/208/1/4

Paxton, B., Marchant, P., Schwab, J., et al. 2015, ApJS, 220, 15, doi: 10.1088/0067-0049/220/1/15

Paxton, B., Schwab, J., Bauer, E. B., et al. 2018, ApJS, 234, 34, doi: 10.3847/1538-4365/aaa5a8

Pedregosa, F., Michel, V., Grisel, O., et al. 2011, Journal of Machine Learning Research, 12, 2825. http://scikit-learn.sourceforge.net.

Pelisoli, I., Bell, K. J., Kepler, S. O., & Koester, D. 2019, MNRAS, 482, 3831, doi: 10.1093/mnras/sty2979

Pelisoli, I., Kepler, S. O., & Koester, D. 2018a, Monthly Notices of the Royal Astronomical Society, 475, 2480, doi: 10.1093/mnras/sty011

Pelisoli, I., Kepler, S. O., Koester, D., et al. 2018b, Monthly Notices of the Royal Astronomical Society, 478, 867, doi: 10.1093/MNRAS/STY1101

Pelisoli, I., Kepler, S. O., Koester, D., & Romero, A. D. 2017, in Astronomical Society of the Pacific Conference Series, Vol. 509, 20th European White Dwarf Workshop, ed. P. E. Tremblay, B. Gaensicke, & T. Marsh, 447. https://arxiv.org/abs/1610.05550

Pelisoli, I., & Vos, J. 2019, MNRAS, 488, 2892, doi: 10.1093/mnras/stz1876

Placco, V. M., Frebel, A., Lee, Y. S., et al. 2015, ApJ, 809, 136, doi: 10.1088/0004-637X/809/2/136

Placco, V. M., Frebel, A., Beers, T. C., et al. 2016, ApJ, 833, 21, doi: 10.3847/0004-637X/833/1/21

Riaz, R., Bovino, S., Vanaverbeke, S., & Schleicher, D. R. G. 2018, MNRAS, 479, 667, doi: 10.1093/mnras/sty1635

Robitaille, T. P., Tollerud, E. J., Greenfield, P., et al. 2013, Astronomy and Astrophysics, 558, 1, doi: 10.1051/0004-6361/201322068

Roederer, I. U., Preston, G. W., Thompson, I. B., et al. 2014, AJ, 147, 136, doi: 10.1088/0004-6256/147/6/136

Ryan, S. G., & Norris, J. E. 1991a, AJ, 101, 1835, doi: 10.1086/115811

—. 1991b, AJ, 101, 1865, doi: 10.1086/115812

Ryan, S. G., Norris, J. E., & Bessell, M. S. 1991, AJ, 102, 303, doi: 10.1086/115878

Salgado, J., González-Núñez, J., Gutiérrez-Sánchez, R., et al. 2017, Astronomy and Computing, 21, 22, doi: 10.1016/j.ascom.2017.08.002

Saumon, D., Bergeron, P., Lunine, J. I., Hubbard, W. B., & Burrows, A. 1994, ApJ, 424, 333, doi: 10.1086/173892

Schatzman, E. 1948, Nature, 161, 61, doi: 10.1038/161061b0

Schlaufman, K. C., Thompson, I. B., & Casey, A. R. 2018, The Astrophysical Journal, 867, 98, doi: 10.3847/1538-4357/aadd97

Silk, J. 1983, MNRAS, 205, 705, doi: 10.1093/mnras/205.3.705

Smee, S. A., Gunn, J. E., Uomoto, A., et al. 2013, AJ, 146, 32, doi: 10.1088/0004-6256/146/2/32

Smith, J. A., Tucker, D. L., Kent, S., et al. 2002, AJ, 123, 2121, doi: 10.1086/339311

Stacy, A., & Bromm, V. 2013, MNRAS, 433, 1094, doi: 10.1093/mnras/stt789

—. 2014, ApJ, 785, 73, doi: 10.1088/0004-637X/785/1/73

Stacy, A., Bromm, V., & Lee, A. T. 2016, MNRAS, 462, 1307, doi: 10.1093/mnras/stw1728

Stacy, A., Greif, T. H., & Bromm, V. 2010, MNRAS, 403, 45, doi: 10.1111/j.1365-2966.2009.16113.x

—. 2012, MNRAS, 422, 290, doi: 10.1111/j.1365-2966.2012.20605.x

Suda, T., Yamada, S., Katsuta, Y., et al. 2011, MNRAS, 412, 843, doi: 10.1111/j.1365-2966.2011.17943.x

Suda, T., Katsuta, Y., Yamada, S., et al. 2008, PASJ, 60, 1159, doi: 10.1093/pasj/60.5.1159

Suda, T., Hidaka, J., Aoki, W., et al. 2017, PASJ, 69, 76, doi: 10.1093/pasj/psx059

Tegmark, M., Silk, J., Rees, M. J., et al. 1997, ApJ, 474, 1, doi: 10.1086/303434

Tremblay, P. E., & Bergeron, P. 2009, Astrophysical Journal, 696, 1755, doi: 10.1088/0004-637X/696/2/1755

Virtanen, P., Gommers, R., Oliphant, T. E., et al. 2020, Nature Methods, 17, 261, doi: 10.1038/s41592-019-0686-2

Wenger, M., Ochsenbein, F., Egret, D., et al. 2000, A&AS, 143, 9, doi: 10.1051/aas:2000332

Wollenberg, K. M. J., Glover, S. C. O., Clark, P. C., & Klessen, R. S. 2020, MNRAS, 494, 1871, doi: 10.1093/mnras/staa289

Yamada, S., Suda, T., Komiya, Y., Aoki, W., & Fujimoto, M. Y. 2013, MNRAS, 436, 1362, doi: 10.1093/mnras/stt1652

Yanny, B., Rockosi, C., Newberg, H. J., et al. 2009, AJ, 137, 4377, doi: 10.1088/0004-6256/137/5/4377

Yong, D., Norris, J. E., Bessell, M. S., et al. 2013, ApJ, 762, 26, doi: 10.1088/0004-637X/762/1/26

Yoon, J., Beers, T. C., Placco, V. M., et al. 2016, The Astrophysical Journal, 833, 20, doi: 10.3847/0004-637x/833/1/20

York, D. G., Adelman, J., Anderson, Jr., J. E., et al. 2000, The Astronomical Journal, doi: 10.1086/301513

Yu, H.-F., Huang, F.-L., & Lin, C.-J. 2011, Machine Learning, 85, 41, doi: 10.1007/s10994-010-5221-8